


**Please cite the Published Version**

Hameed, Marwah A, Ibrahim, Ghalib R and Albarbar, A  (2020) Effect of friction and shear strength enhancement on delamination prediction. Journal of Composite Materials, 54 (23). pp. 3329-3342. ISSN 0021-9983

**DOI:** <https://doi.org/10.1177/0021998320911719>

**Publisher:** SAGE Publications

**Version:** Accepted Version

**Downloaded from:** <https://e-space.mmu.ac.uk/625497/>

**Usage rights:**  In Copyright

**Additional Information:** This is an Author Accepted Manuscript of a paper accepted for publication in Journal of Composite Materials, published by and copyright Sage.

**Enquiries:**

If you have questions about this document, contact [openresearch@mmu.ac.uk](mailto:openresearch@mmu.ac.uk). Please include the URL of the record in e-space. If you believe that your, or a third party's rights have been compromised through this document please see our Take Down policy (available from <https://www.mmu.ac.uk/library/using-the-library/policies-and-guidelines>)

# Effect of Friction and Shear Strength Enhancement on Delamination Prediction

Marwah A Hameed<sup>1,\*</sup>, Ghalib R. Ibrahim<sup>2</sup>, A. Albarbar<sup>2</sup>,

*1 School of Mechanical, Aerospace and Civil Engineering, The University of Manchester, Manchester, M13 9PL, UK.*

*2 Department of Engineering, Manchester Metropolitan University, Manchester M1 5GD, UK.*

## Abstract

This study introduces intra-laminar damage mode in composite structures and its effect on delamination prediction. The progressive damage models for the matrix cracking and fibre failure are only available to shell element in ABAQUS based on Hashin's Model. The results showed that the predicted matrix cracking based on damage model presently available in ABAQUS diverged from the experimental data. Therefore, a new model based on strain failure criteria was developed which can be used to both shell element and 3-D solid element.

The effect of friction coefficient and enhancement factor on the delamination lobes within the delamination area were also investigated. It can be observed that the intact zone can be captured in laminate  $[0_3/90_3]_s$  and  $[90_3/0_3]_s$  which subjected under low velocity impact when using enhancement factor ( $\eta=0.75$ ) and friction coefficient ( $\geq 0.5$ ) together with the developed approach.

## 1. Introduction

In laminated composites, damage that develops internally invariably presents itself as complex patterns that are difficult to detect (Y. Shi 2016). Every ply in the composite laminate will share the applied load depending on its location, orientation, stiffness and stacking sequence. When a composite laminate fails, the failure will occur ply by ply. Once an individual ply has failed, the load is shared between the remaining plies which are then, individually, subjected to greater load, and so on until every ply has failed (Murugesan and Rajamohan 2017). Generally, composite materials fail due to both intra- and inter-laminar failure. Intra-laminar failure can occur within single ply as breakage of the fibres, or will take the form of compressive and tensile damage in the matrix. Failure between neighbouring plies is called inter-laminar (delamination) failure. The consequent intra- and inter-laminar failure damage modes are found to interact with each other as the damage progresses. For example, within

composite laminated structures the initial damage modes are due to their characteristics being resin dominated, resulting in cracking of the transverse matrix in a direction parallel to the fibres. The consequence is the degradation of both strength and stiffness of the composite materials but, usually, the composite laminate can carry the load if the fibres do not break. A stress concentration will be generated at an interface due to crack propagation in the matrix to the interface between plies. This stress concentration leads to the development of delamination. The finally failure of the laminated composites are usually caused by the fibre failure. Low energy impacts generate impact damage that is barely visible and may not be easy to detect, but which is a serious issue when designing and manufacturing composite structural components. It is necessary to research into the different damage modes to better understand the interactions that occur during likely failure processes in composite laminated structures, enhancing the resistance to damage in composites subjected to low-velocity impacts by optimising the lay-up configuration. The steps required for the analysis of progressive ply failure include: analysis of stresses developed in the laminate and their distribution for the specified load and given boundary conditions; assessing a failure by applying appropriate failure criterion to explain the failure that has occurred, whether delamination, fibre, or failed matrix; applying appropriate stiffness or material degradation criteria. These steps are applied repeatedly for each and every failure until the very last ply of the composite laminate fails (Murugesan and Rajamohan 2017).

## 2. Progressive Damage in ABAQUS Based on Hashin's Model

Hashin's theory (Hashin 1980) has been used in ABAQUS software to predict the damage onset in unidirectional fibre-reinforced composites. These criteria are known as separate mode criteria because they classify damage into four different damage initiation mechanisms; fibre tension, fibre compression, matrix tension, and matrix compression. The initiation criteria are written generally as:

*Tensile fibre failure* ( $\sigma_{11} > 0$ )

$$\left(\frac{\sigma_{11}}{X_T}\right)^2 + \alpha \frac{\tau_{12}^2}{S_L^2} = \begin{cases} \geq 1 & \text{failure} \\ < 1 & \text{no failure} \end{cases} \quad (1)$$

*Compressive fibre failure* ( $\sigma_{11} < 0$ )

$$\left(\frac{\sigma_{11}}{X_C}\right)^2 = \begin{cases} \geq 1 & \text{failure} \\ < 1 & \text{no failure} \end{cases} \quad (2)$$

*Tensile matrix failure*  $\sigma_{22} > 0$

$$\left(\frac{\sigma_{22}}{Y_T}\right)^2 + \frac{\tau_{12}^2}{S_L^2} = \begin{cases} \geq 1 & \text{failure} \\ < 1 & \text{no failure} \end{cases} \quad (3)$$

*Compressive matrix failure when  $\sigma_{22} < 0$*

$$\left(\frac{\sigma_{22}}{2S_T}\right)^2 + \left(\frac{\sigma_{22}}{Y_C}\right) \left[ \left(\frac{Y_C}{2S_T}\right)^2 - 1 \right] + \frac{\tau_{12}^2}{S_L^2} = \begin{cases} \geq 1 & \text{failure} \\ < 1 & \text{no failure} \end{cases} \quad (4)$$

where  $\sigma_{11}$  is the stress in the direction of the fibres,  $\sigma_{22}$  is the stress in the direction perpendicular to the fibres,  $X_T$  is the tensile strength and  $X_C$  is the compressive strength in the direction of the fibres,  $Y_T$  is the tensile strength and  $Y_C$  is the compressive strength in the direction perpendicular to the fibres (transverse).  $S_L$  and  $S_T$  denote the longitudinal and transverse shear strength respectively.

The coefficient  $\alpha$  in the tensile fibre failure equation is used to take into consideration the contribution of the shear stress. In ABAQUS, the coefficient  $\alpha$  is set to zero ( $\alpha = 0$ ) to obtain the model proposed by Hashin and Rotem or  $\alpha$  is set to unity ( $\alpha = 1$ ) to obtain the proposed model by Hashin.

After damage initiation, the stiffness of the material will be degraded if the structure undergoes further loading. To control the reduction of the stiffness, damage parameters are introduced and their values are assumed to be in the range of zero (undamaged) to unity (fully damaged). ABAQUS adopts the following expression in order to evaluate the degradation in the material stiffness caused by each failure mode.

$$d_k = \frac{\delta_{eq,k}^f (\delta_{eq,k} - \delta_{eq,k}^0)}{\delta_{eq,k} (\delta_{eq,k}^f - \delta_{eq,k}^0)} \quad (5)$$

where  $\delta_{eq} = \sqrt{\langle \delta_1 \rangle^2 + \delta_2^2 + \delta_3^2}$  is the equivalent displacement.

$\delta_{eq}^0$  is the critical equivalent displacement at damage initiation, and  $\delta_{eq,k}^f = 2G_{k,C}/\sigma_k$  refers to the equivalent displacement at full failure. This formula has been used to calculate damage of fibre and matrix under tension or compression, thus, in the damage parameter equation,  $k \in (ft, fc, mt, mc)$  and  $\sigma_k \in (X_T, X_C, Y_T, Y_C)$

### 3. Present Proposed Method Based on Strain Failure Criteria

The Hashin's damage model in ABAQUS is only applicable to shell or continuum shell

elements. In some scenarios, e.g. impact loading, the through-thickness stress must be considered, and 3D analysis performed in order to obtain satisfactory simulation. Therefore a 3D damage model is developed to take the through thickness stress into consideration when using solid element in the finite element model.

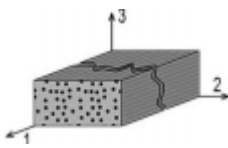
### 3.1 Damage Initiation Criteria

A succinct 3-D strength criterion has been developed by (Liu et al. 2014) based on the work by (Linde and de Boer 2006). This criterion has been successfully used to predict the different damage modes in composites: both fibre and matrix damage. Figure 1 shows different criterion representing the different damage modes; where  $\varepsilon_{ij}$ , ( $i, j = 1, 2$  and  $3$ ) represents the strain component in direction ( $i, j$ ). Whereas a superscript ( $c$ ,  $s$  or  $t$ ) represents the strain limit for compression, shear or tension, respectively.

If any of the terms on the left side of either criterion is greater than or equal to unity, then corresponding damage will occur and the level of damage can be evaluated according to the level of the strain. Most non-linear calculations in mechanics use incremental increases in the strain for iteration purposes, which facilitates non-linear iterations. Note that this criterion can differentiate between different damage modes. This makes it feasible to decrease the stiffness of the material and assess the effect of each different damage mode.

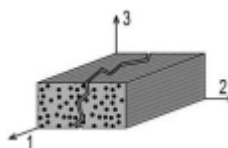
The criteria presented in Figure 1 contain not only linear and quadratic terms but also combinations of compression and tension effects, which should improve the accuracy of the criteria (Liu et al. 2014).

Fibre damage



$$\frac{\varepsilon_{11}}{\varepsilon_{11}^t} - \frac{\varepsilon_{11}}{\varepsilon_{11}^c} + \frac{\varepsilon_{11}^2}{\varepsilon_{11}^t \varepsilon_{11}^c} \geq 1$$

Matrix damage



$$\frac{\varepsilon_{22}}{\varepsilon_{22}^t} - \frac{\varepsilon_{22}}{\varepsilon_{22}^c} + \frac{\varepsilon_{12}^2}{(\varepsilon_{12}^s)^2} + \frac{\varepsilon_{22}^2}{\varepsilon_{22}^t \varepsilon_{22}^c} \geq 1$$

Figure **Error! No text of specified style in document.**1 Criteria for fibre and matrix failures (Liu et al. 2014)

The equation representing the criterion for fibre failure can be re-arranged to distinguish between tension failure ( $Ff_t$ ) and compression failure ( $Ff_c$ ). Failure of a fibre is initiated if either failure index  $Ff_t$  or  $Ff_c$  exceeds the failure strain  $\varepsilon_{11}^t$  or  $\varepsilon_{11}^c$  respectively.

$$Ff_t^2 = \varepsilon_{11}\varepsilon_{11}^t - \frac{\varepsilon_{11}(\varepsilon_{11}^t)^2}{\varepsilon_{11}^c} + \frac{\varepsilon_{11}^2\varepsilon_{11}^t}{\varepsilon_{11}^c} \geq (\varepsilon_{11}^t)^2 \quad (\text{Fibre tension failure}) \quad (6)$$

$$Ff_c^2 = \frac{\varepsilon_{11}(\varepsilon_{11}^c)^2}{\varepsilon_{11}^t} - \varepsilon_{11}\varepsilon_{11}^c + \frac{\varepsilon_{11}^2\varepsilon_{11}^c}{\varepsilon_{11}^t} \geq (\varepsilon_{11}^c)^2 \quad (\text{Fibre compression failure}) \quad (7)$$

Here  $\varepsilon_{11}$  represents the strain component in the fibre direction.  $\varepsilon_{11}^c$  and  $\varepsilon_{11}^t$  are the fibre failure strains in the fibre direction, for compression and tension, respectively. These may be found from:

$$\varepsilon_{11}^t = \frac{X_t}{E_{11}} \quad (8)$$

$$\varepsilon_{11}^c = \frac{X_c}{E_{11}} \quad (9)$$

where  $X_t$  and  $X_c$  are the tensile and compressive strength respectively, both measured in the direction of the fibre.

Similarly, for matrix failure, tension failure ( $Mf_t$ ) and compression failure ( $Mf_c$ ) are initiated when:

$$Mf_t^2 = \varepsilon_{22}\varepsilon_{22}^t - \frac{\varepsilon_{22}(\varepsilon_{22}^t)^2}{\varepsilon_{22}^c} + \frac{\varepsilon_{12}^2(\varepsilon_{22}^t)^2}{(\varepsilon_{12}^s)^2} + \frac{\varepsilon_{22}^2\varepsilon_{22}^t}{\varepsilon_{22}^c} \geq (\varepsilon_{22}^t)^2 \quad (10)$$

$$Mf_c^2 = \frac{\varepsilon_{22}(\varepsilon_{22}^c)^2}{\varepsilon_{22}^t} - \varepsilon_{22}\varepsilon_{22}^c + \frac{\varepsilon_{12}^2(\varepsilon_{22}^c)^2}{(\varepsilon_{12}^s)^2} + \frac{\varepsilon_{22}^2\varepsilon_{22}^c}{\varepsilon_{22}^t} \geq (\varepsilon_{22}^c)^2 \quad (11)$$

where  $\varepsilon_{12}$  and  $\varepsilon_{22}$  are the strain components in the shear direction and normal to the fibre direction, respectively.  $\varepsilon_{12}^s$  is the shear failure strain and  $\varepsilon_{22}^t$  and  $\varepsilon_{22}^c$  are the tensile and compressive failure strains perpendicular to the direction of the fibre, respectively. These may be found from:

$$\varepsilon_{22}^c = \frac{Y_c}{E_{22}} \quad (12)$$

$$\varepsilon_{22}^t = \frac{Y_t}{E_{22}} \quad (13)$$

$$\varepsilon_{12}^s = \frac{S_{12}}{G_{12}} \quad (14)$$

where  $Y_c$  and  $Y_t$  are the compressive and tensile strengths in the transverse direction respectively, and  $S_{12}$  is the longitudinal shear strength.

### 3.2 Damage Evolution Law

When predicting the likely damage in composite laminated structures, it usual needs to define a law or rule which controls the damage evolution. This law will, usually, define the degradation of the stiffness of the material depending on the damage mode. In order to predict the development of the damage, one of the most convenient approaches is to introduce and apply a degradation parameter correlated with that particular failure mode.

Modelling damage evolution invariably includes the assumption that damage will be followed by ongoing degradation of e.g., the stiffness of the material, and eventual material failure. Non-linearity is assumed for shear loading as well as for both compressive and tensile loadings in the matrix, and along the direction of the fibre. When used for modelling stress softening, the results will be mesh-dependent; the calculated value of the energy dissipated will decrease with reduction in the mesh size, or dimensions of the element. To overcome this problem and reduce sensitivity to the mesh size, characteristic length and energy dissipation are included in the law defining damage evolution, see Equations (4.29)-(4.32), (Guo et al. 2013).

A damage variable,  $D$ , is introduced. This is a composite function of: stiffness of the undamaged material, the value of a “failure initiation variable” which depends on the mode and extent of the failure, and the strain at failure. To further reduce sensitivity of the numerical model to mesh size the damage calculations also include matrix and fibre fracture energies ( $G_{mt}$ ,  $G_{mc}$ ,  $G_{ft}$  and  $G_{fc}$ ) and the characteristic length of the element ( $L_c$ ). The matrix damage,  $D_m$ , and the fibre damage,  $D_f$ , take place in directions normal, and parallel to the fibres, respectively. The corresponding values may be found in (Naderi and Khonsari 2013):

$$\text{Matrix compression failure } D_{m_c} = 1 - (\varepsilon_{22}^c / M_{f_c}) \exp\left(\frac{-C_{22}(\varepsilon_{22}^c)^2 L_c}{G_{mc}} \left[\frac{M_{f_c}}{\varepsilon_{22}^c} - 1\right]\right) \quad (15)$$

$$\text{Matrix tension failure } D_{m_t} = 1 - (\varepsilon_{22}^t / M_{f_t}) \exp\left(\frac{-C_{22}(\varepsilon_{22}^t)^2 L_c}{G_{mt}} \left[\frac{M_{f_t}}{\varepsilon_{22}^t} - 1\right]\right) \quad (16)$$

$$\text{Fibre tension failure } D_{f_t} = 1 - (\varepsilon_{11}^t / F_{f_t}) \exp\left(\frac{-C_{11}(\varepsilon_{11}^t)^2 L_c}{G_{ft}} \left[\frac{F_{f_t}}{\varepsilon_{11}^t} - 1\right]\right) \quad (17)$$

$$\text{Fibre compression failure } D_{f_c} = 1 - (\varepsilon_{11}^c / F_{f_c}) \exp\left(\frac{-C_{11}(\varepsilon_{11}^c)^2 L_c}{G_{fc}} \left[\frac{F_{f_c}}{\varepsilon_{11}^c} - 1\right]\right) \quad (18)$$

The damage parameters for the fibre damage and matrix damage are defined as (Du et al. 2016):

$$D_f = 1 - (1 - Df_t)(1 - Df_c) \quad (19)$$

$$D_m = 1 - (1 - Dm_t)(1 - Dm_c) \quad (20)$$

$D_f$  and  $D_m$  lie in the range  $[0, 1]$ , where  $D_f = D_m = 0$  corresponds to no damage, and  $D_f = D_m = 1$  corresponds to full damage.

The stiffness matrix of the material then becomes (Guo et al. 2013):

$$C_{11}^d = (1 - D_f)C_{11} \quad (21)$$

$$C_{22}^d = (1 - D_m)C_{22} \quad (22)$$

$$C_{12}^d = (1 - D_f)(1 - D_m)C_{12} \quad (23)$$

$$C_{13}^d = (1 - D_f)C_{13} \quad (24)$$

$$C_{23}^d = (1 - D_f)(1 - D_m)C_{23} \quad (25)$$

$$C_{44}^d = (1 - D_f)(1 - D_m)C_{44} \quad (26)$$

Thus, the effective stiffness matrix,  $C^d$ , including the effect of the damage on the material stiffness (after damage has been initiated at a point), can be written as:

$$C^d = \begin{bmatrix} (1 - D_f)C_{11} & (1 - D_f)(1 - D_m)C_{12} & (1 - D_f)C_{13} & 0 & 0 & 0 \\ (1 - D_f)(1 - D_m)C_{12} & (1 - D_m)C_{22} & (1 - D_f)(1 - D_m)C_{23} & 0 & 0 & 0 \\ (1 - D_f)C_{13} & (1 - D_f)(1 - D_m)C_{23} & C_{33} & 0 & 0 & 0 \\ 0 & 0 & 0 & (1 - D_f)(1 - D_m)C_{44} & 0 & 0 \\ 0 & 0 & 0 & 0 & C_{55} & 0 \\ 0 & 0 & 0 & 0 & 0 & C_{66} \end{bmatrix} \quad (27)$$

The stress is then updated using:

$$\sigma = C^d \varepsilon \quad (28)$$

By differentiating this expression one can obtain the Jacobian matrix:

$$\frac{\partial \sigma}{\partial \varepsilon} = C^d + \frac{\partial C^d}{\partial \varepsilon} : \varepsilon \quad (29)$$

### 3.3 Implementing the Proposed Damage Model in ABAQUS

The above damage model for intra-laminar fibre and matrix failure has been implemented in ABAQUS software via UMAT (User Material Subroutine). This simple subroutine is applicable to both continuum shell and 3-D solid elements. The subroutine assumes the fibre direction is along the local x-direction. Thus, when continuum shell or 3-D solid elements are used, but the local direction of the fibre is not aligned with the global X-direction, it is necessary to specify the local orientation of the material.  $Dm$  and  $Df$  are stored as solution-dependent



variables (Du et al. 2016). The UMAT subroutine flowchart used to update and evaluate damage, and calculate strains and stresses is shown in Figure 2.

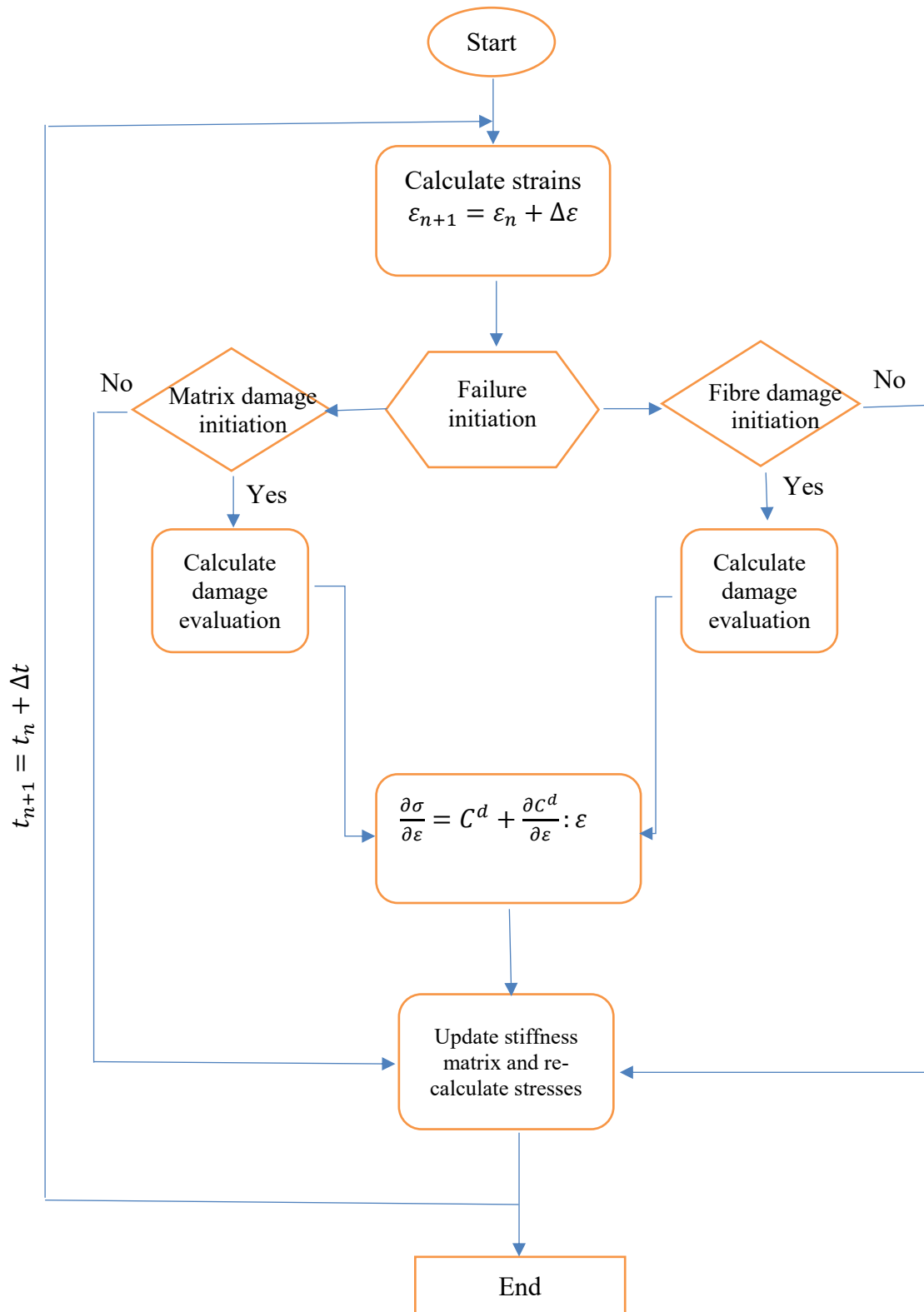


Figure Error! No text of specified style in document.2 Flowchart for UMAT subroutine

#### 4. Simulating Impact Damage in Composite Laminates

To validate the proposed damage models, impact tests available in the literature were modelled and predicted results of damage were compared with experimental observation.

##### 4.1 Description of Impact Test on Composite Laminates as Reported in the Literature

(Aymerich et al. 2009) carried out drop weight impact tests on  $[0_3/90_3]_s$  and  $[90_3/0_3]_s$  graphite /epoxy composite laminates. The properties of the graphite /epoxy composite is listed in Table 1

Table **Error! No text of specified style in document.**1 Properties of graphite/epoxy laminate used in tests (Aymerich et al. 2009)

Property	Carbon /epoxy laminate
Longitudinal Young's modulus	$E_1 = 93.7 * 10^9 Pa$
Transverse Young's modulus	$E_2 = E_3 = 7.45 * 10^9 Pa$
Shear modulus	$G_{12} = G_{13} = G_{23} = 3.97 * 10^9 Pa$
Poisson's ratio	$\nu_{12} = \nu_{13} = \nu_{23} = 0.261$
Longitudinal tensile strength	$X_T = 1850 MPa$
Longitudinal compressive strength	$X_C = 1470 MPa$
Transverse tensile strength	$Y_T = 30 MPa$
Transverse compressive strength	$Y_C = 140 MPa$
Shear strength	$S = 80 MPa$
Density	$\rho = 1600 kg/m^3$

(Aymerich et al. 2009) used rectangular shaped specimens of the laminate, 65 mm x 87.5 mm, and 2 mm thick, see Figure 4.3. An impact test machine was used with a falling mass of 2.3 kg with a hemispherical steel nose of 12.5 mm diameter. To avoid more than a single impact on the test specimen, the impact mass was captured after the initial rebound by using a pneumatic braking system.

The specimens were simply supported along all edges, on a horizontal, flat, steel plate with a 45 mm x 67.5 mm rectangular opening. Impact energies in the range of 0.5 J to 7J were obtained by changing the drop height of the impacting mass (with measured impact velocities of between 0.7 m/s and 2.5 m/s).

The induced damage in the composite laminated structures is, typically, a mixture of different

types of fracture events, each with its own complicated 3-D morphology. To discover the contrast between the damaged and undamaged areas of the sample, an X-ray technique was used. In this way a comprehensive assessment of failure in impacted laminates was obtained. Every specimen was scanned over both sides, and the obtained information was combined to give a good assessment. For relatively simple structures such as  $[0_3/90_3]_s$  and  $[90_3/0_3]_s$  composite laminates, delaminations occur, at most, at two interfaces, thus this method provided a complete picture of the through thickness delamination patterns. Typical detected damage in laminate  $[0_3/90_3]_s$  is shown in Figure 3 (Aymerich et al. 2009). A peanut shape delamination grows at the lowermost 90/0 interface along the major axis (fibre direction) of the lower ply. However, there is an intact zone between the lobes of delamination. This intact zone is just underneath the impactor where there is through thickness compression. Experimental results showed that intra-laminar damage develops in the  $0^0$  layers farthest from the impact face as a major bending matrix crack.

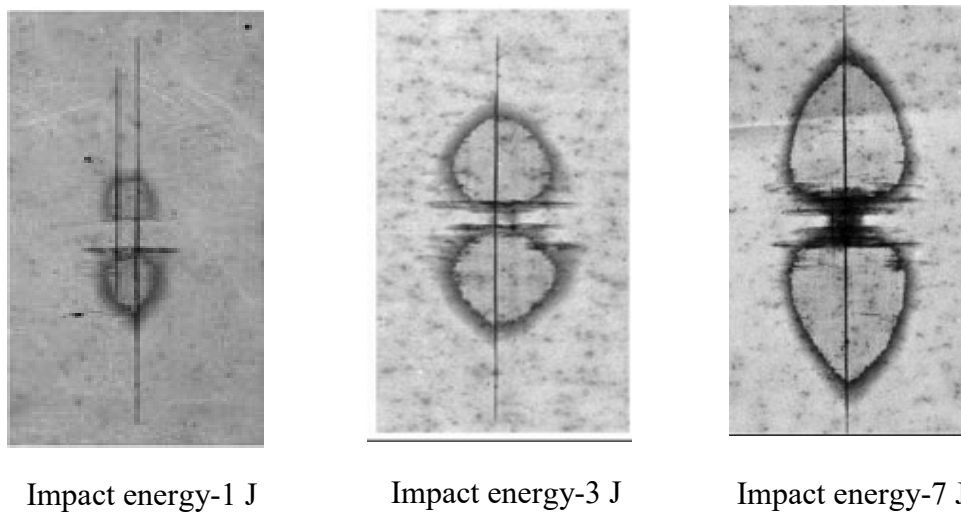


Figure 3 Damage in laminate  $[0_3/90_3]_s$  from experimental results of (Francesconi and Aymerich 2017)

#### 4.2 Creation of FE Model of the Impact Test

ABAQUS was used to model the impact test described above. Intra-laminar damage was modelled using the damage models in ABAQUS and the present proposed model implemented in ABAQUS. The laminate layers were divided into three groups in the thickness direction according to the layer stacking sequences: the first (bottom) consisted of 3 layers at  $0^0$ , the second of six layers at  $90^0$ , and then the top stratum was three layers again at  $0^0$ . A cohesive

layer was placed between the strata with different fibre orientations, the first layer was at the  $[0_3/90_3]$  interface; the second layer was at the  $[90_3/0_3]$  interface. And vice-versa for laminate  $[90_3/0_3]_s$ . Only a quarter of the laminate was modelled due to symmetry.

To connect cohesive interface elements and solid layers in the simulation, a ‘Tie’ constraint was used. The impactor was modelled as an analytical rigid body, because its deformation is so much smaller than that of the composite laminated structures. Such an approximation speeds up the numerical analysis and significantly reduces the computation time. Surface-to-surface contact pairs were used as part of the simulation of the interaction between plate and impactor. This was implemented using a penalty approach. During contact Coulomb friction was applied and the coefficient of friction was set to 0.3.

(Aymerich et al. 2009) identified the parameters which define the behaviour of the cohesive interface. They compared experimental data obtained by static fracture tests, for Mode I (Double Cantilever Beam) and Mode II (End-Notched Flexure) on unidirectional laminates, with simulation results. Table 2 shows cohesive interface properties as found by (Aymerich et al. 2009) for graphite/epoxy laminates.

Table 2 Interface properties as found by (Aymerich et al. 2009)

Initial stiffness	$k_1 = 1.2 * 10^{14} \text{ N/m}^3, k_2 = k_3 = 0.43 * 10^{14} \text{ N/m}^3$
Nominal strength	$\tau_{1c} = 30 * 10^6 \text{ N/m}^2, \tau_{2c} = \tau_{3c} = 80 * 10^6 \text{ N/m}^2$
Mode I fracture toughness	$G_{IC} = 520 \text{ J/m}^2$
Mode II fracture toughness	$G_{IIC} = 970 \text{ J/m}^2$

The cohesive model developed to take into account the enhancing effect of through thickness compression on Mode II (in-plane shear) fracture. The enhancement of interfacial shear strength in the damage model is defined as (Zou and Hameed 2018);

$$\tau_{2cn} = (1 - \eta \frac{\tau_1}{\tau_{2c}}) \tau_{2c} \quad (30)$$

where  $\tau_{2cn}$  is an enhanced shear strength and  $\eta$  is an enhancement factor to take account of the through-thickness compression.  $\tau_{2c}$  is interface shear strength of Mode II.  $\tau_1$  is shear stress of Mod I.

The use of this type of cohesive zone model is necessary in the present case as impact produces significant through thickness compression in the laminate in the area underneath the impactor. The enhancement factor ( $\eta$ ), which determines the effect of compressive stress on the Mode II delamination resistance, was given a value of ( $\eta=0.75$ ) (Francesconi and Aymerich 2017).

### 4.3 Predicted Damage Using Hashin's Damage Model in ABAQUS

Hashin's damage model was first employed to simulate the intra-laminar damage in the laminate. The three groups of composite layers were modelled by the continuum shell element SC8R, because Hashin's damage model in ABAQUS is only applicable to shell elements. The cohesive element employed in the simulation was the eight-node three-dimensional cohesive element COH3D8. A fine mesh (0.25 mm x 0.25 mm) was used. The predicted matrix cracking in each layer under impact energy of 7J is shown in Figure 4, while Figure 5a presents the development of matrix cracking in the 0° layer nearest to the support of laminate  $[0_3/90_3]_s$  under different impact energies (1J, 3J and 7J). The predicted matrix cracking was compared with the experimental findings. It is shown that the predicted matrix cracking from Hashin's damage model diverged from the experimental results. Therefore, the proposed damage model to simulate intra-laminar damage is introduced in the next section.

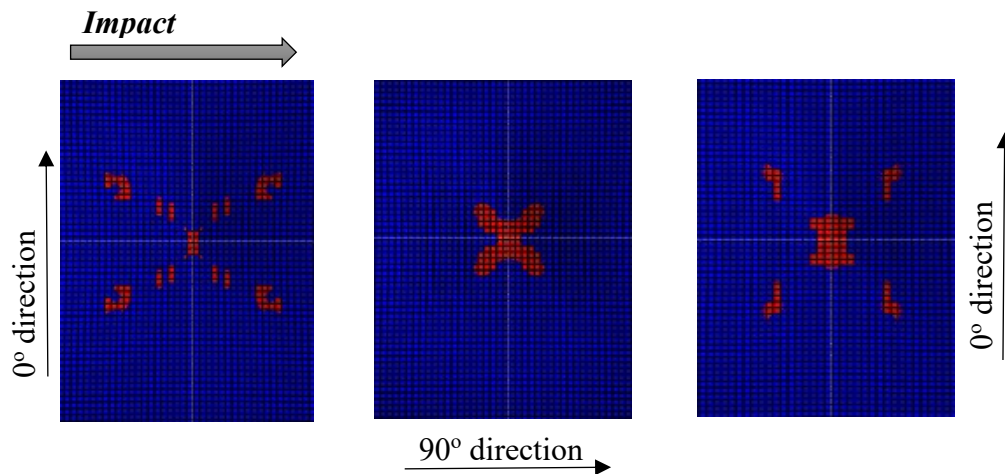


Figure Error! No text of specified style in document. Matrix cracking at each layer in laminate  $[0_3/90_3]_s$  under impact energy 7J

The predicted delamination of laminate  $[0_3/90_3]_s$  under different impact energies (1J, 3J and 7J) is shown in Figure 4.7b. There is a small intact zone in the predicted delamination when the impact energy level is low. However, this intact zone disappears with high impact energy, although a high friction coefficient (0.9) was used. This is because of the Hashin's damage model in ABAQUS can be applied when using shell or continuum shell element. Therefore, in some loading conditions, e.g. low impact loading, the stress along thickness direction must be taken into account, and 3D analysis implemented in order to get satisfactory results.

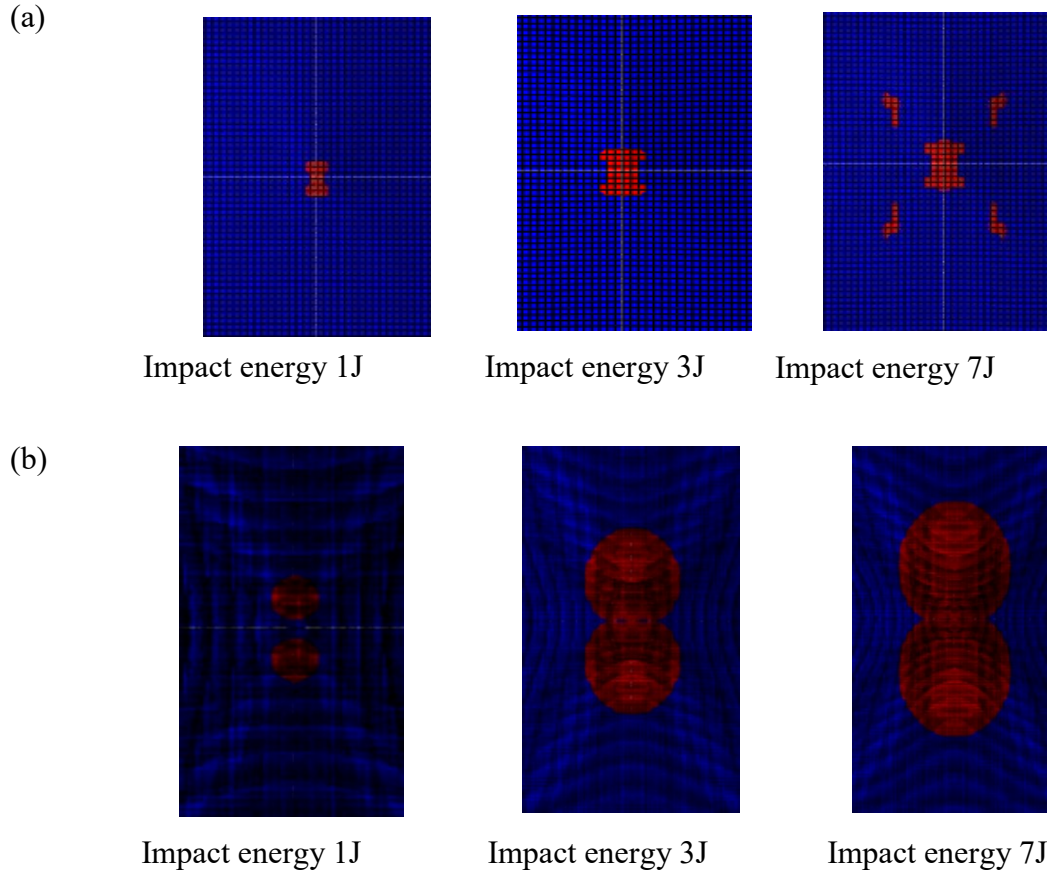


Figure 5 (a) Predicted matrix cracking (b) delamination in laminate  $[0_3/90_3]_s$  using Hashin model (friction is included)

#### 4.4 Predicted Damage Using the Proposed Damage Model

The three groups of composite layers were modelled by the solid element C3D8 when the present intra-laminar damage model was applied. Figure 6 illustrates the simulation results of matrix cracking in each layer under high impact energy (7J). Figure 7 shows delamination development at the uppermost interface in laminate the  $[0_3/90_3]_s$  under various impact energies.

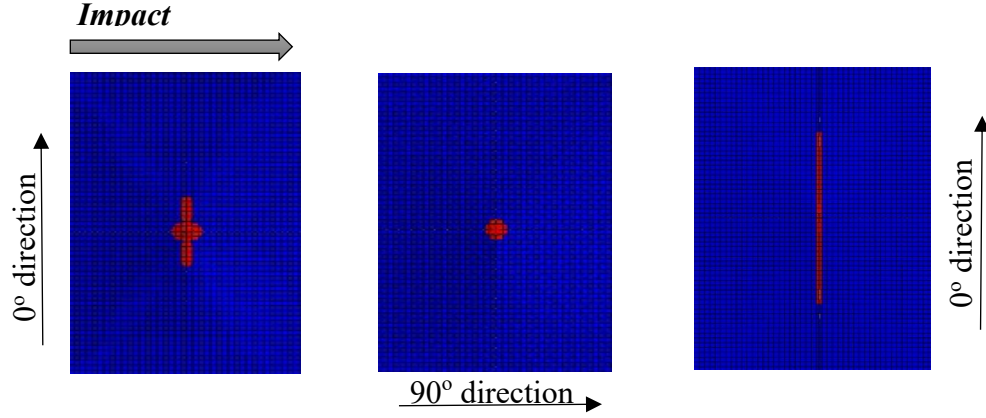


Figure 6 Matrix cracking at each layer in laminate  $[0_3/90_3]_s$  under impact energy 7J

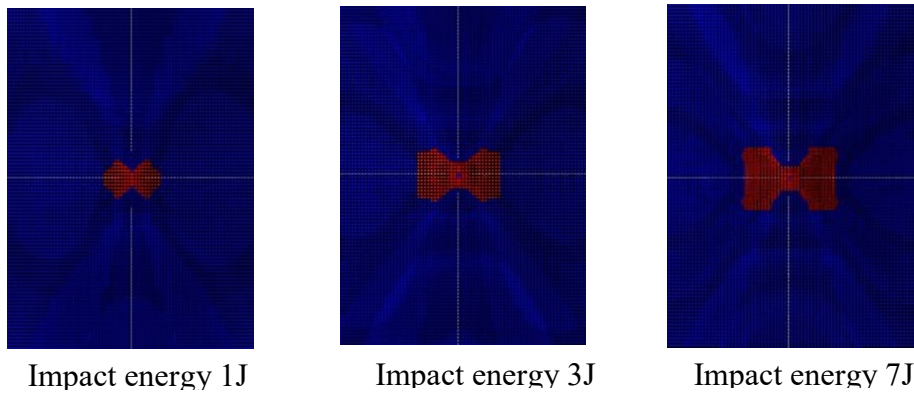


Figure 7 Delamination development at uppermost interface in laminate  $[0_3/90_3]_s$

Figures 8a and 9 show the developing intra-laminar damage in the lower layer of laminate  $[0_3/90_3]_s$  and laminate  $[90_3/0_3]_s$  using present proposed method based on strain failure criteria. As expected the damage grows along the fibre direction, and develops with increase in impact energy. The predicted matrix cracking area is in good agreement with the experimental observation. This proves that the present intra-laminar damage model provides much better predictions than the existing intra-laminar damage model in ABAQUS.

Figures 8b and 10 display the delamination at the lowermost interface when friction coefficient is ( $f_c = 0.9$ ) and enhancement factor is ( $\eta = 0.75$ ). The numerical results revealed that the intact zone for delamination is captured and there is a good agreement with the experimental measured delamination images from (Aymerich et al. 2009).



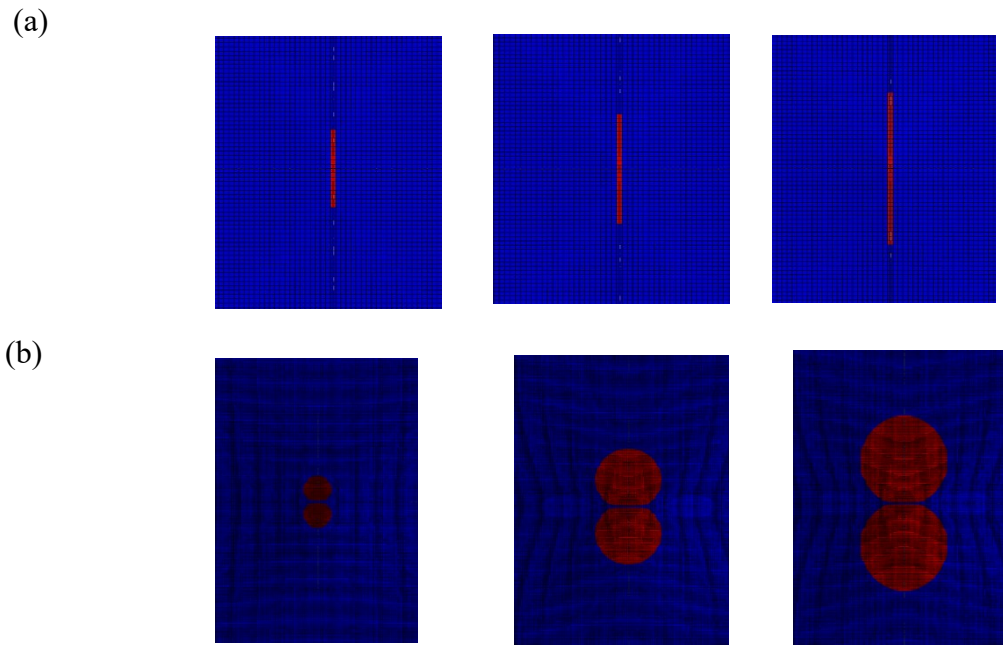


Figure 8 (a) Predicted matrix cracking (b) delamination in laminate  $[0_3/90_3]_s$  using proposed model (friction  $f_c = 0.9$  and  $\eta = 0.75$ )

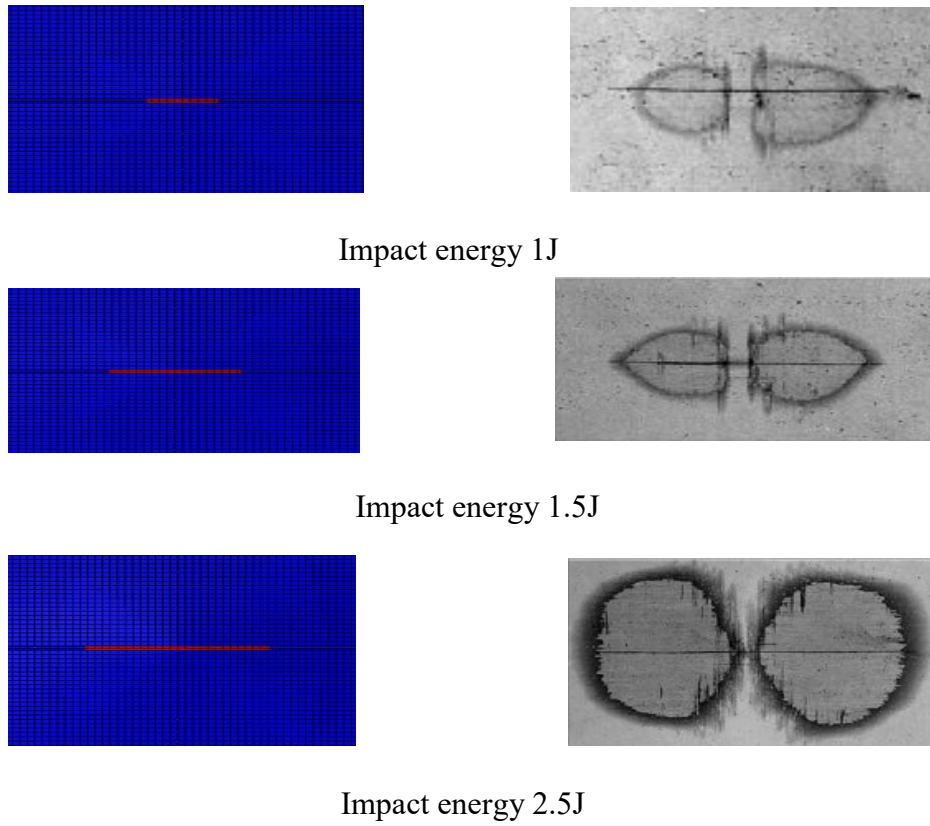
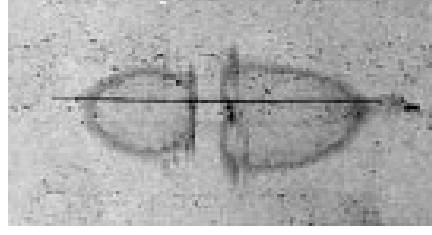
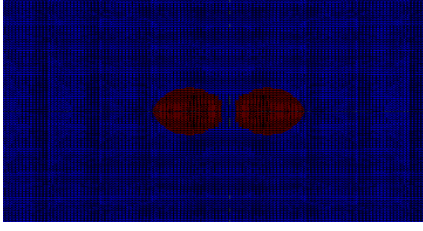
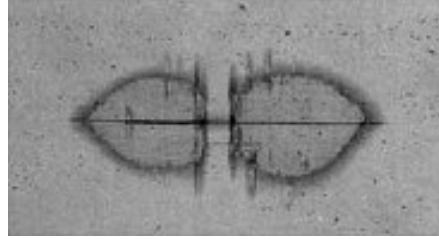
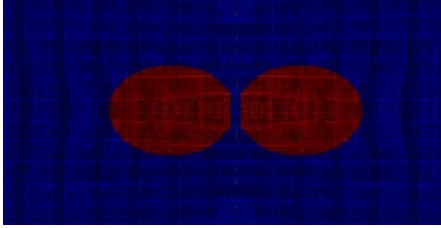


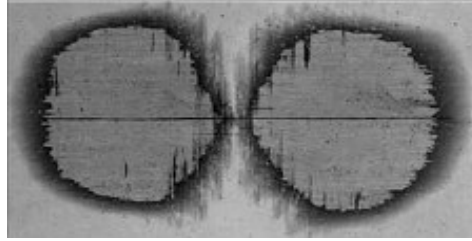
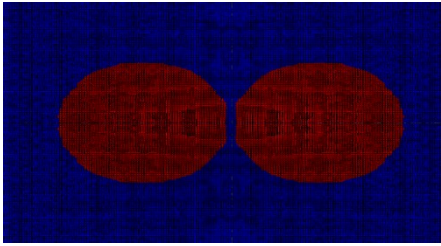
Figure 9 Matrix cracking in laminate  $[90_3/0_3]_s$  using proposed model (friction  $f_c = 0.9$  and  $\eta = 0.75$ ) with three levels of impact energy



Impact energy 1J



Impact energy 1.5J



Impact energy 2.5J

Figure 10 Delamination in laminate  $[90_3/0_3]_s$  using proposed model (friction  $f_c = 0.9$  and  $\eta = 0.75$ ) with three levels of impact energy

#### 4.4.1 Effect of Matrix Cracking on Delamination Prediction

The interaction between matrix cracking and delamination was also investigated. Simulations were performed in two cases, without and with consideration of matrix cracking. The results show that the gap between the delamination lobes disappears if the matrix cracking is excluded from the numerical model, see Figures 11 and 13.

This indicates that there is a strong interaction between matrix cracking and delamination. The inclusion of the intra-laminar damage model has the potential for effectively capturing the intact zone in laminate  $[0_3/90_3]_s$  and laminate  $[90_3/0_3]_s$  as illustrated in Figures 12 and 14.

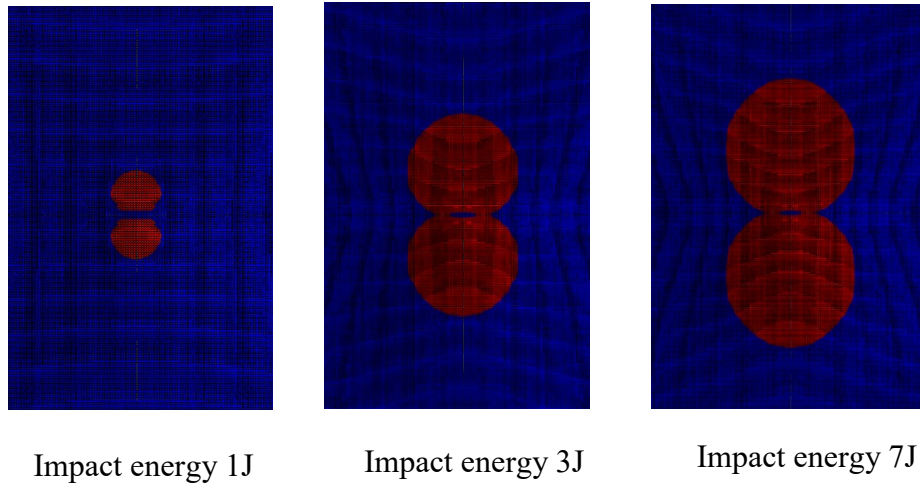


Figure 11 Delamination shape in laminate  $[0_3/90_3]_s$  using proposed model (friction  $f_c = 0.9$  and  $\eta = 0.75$ ) without matrix cracking

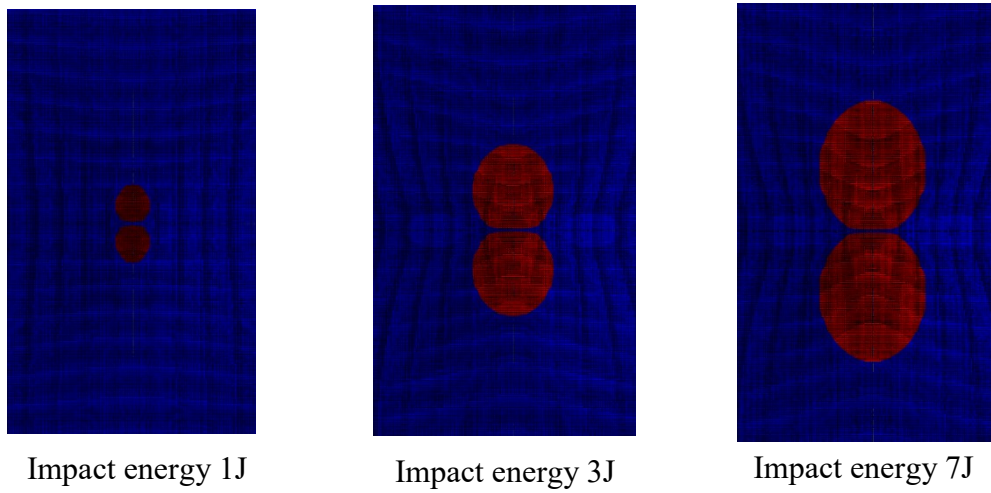


Figure 12 Delamination shape in laminate  $[0_3/90_3]_s$  using proposed model (friction  $f_c = 0.9$  and  $\eta = 0.75$ ) with matrix cracking

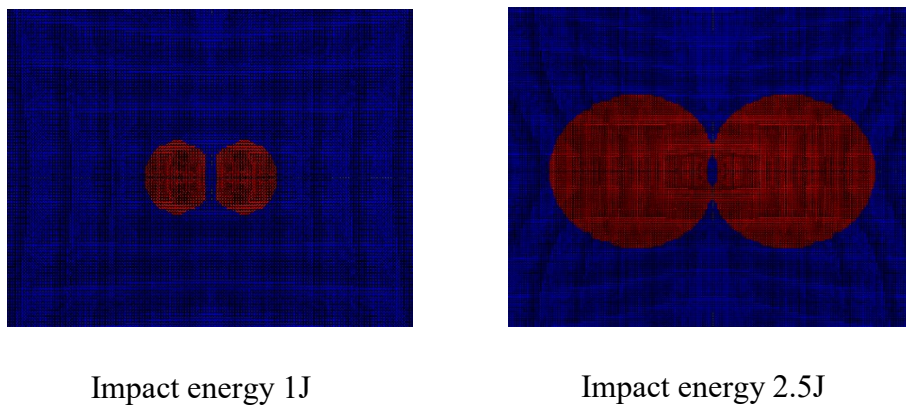


Figure 13 Delamination shape in laminate  $[90_3/0_3]_s$  using proposed model (friction  $f_c = 0.9$  and  $\eta = 0.75$ ) without matrix cracking

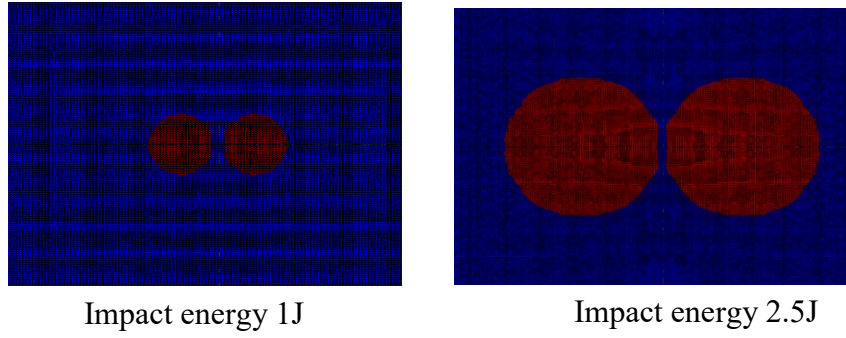


Figure 14 Delamination shape in laminate  $[90_3/0_3]_s$  using proposed model (friction  $f_c = 0.9$  and  $\eta = 0.75$ ) with matrix cracking

#### 4.4.2 Effect of Friction on Model Predictions

As mentioned previously, the fine mesh (0.25 mm x 0.25 mm) should be used to give a smoother delamination contour and improve the predictions of damage, in particular, the intact zone between the lobes of delamination.

Friction in the delaminated area may also contribute to the formation of the intact zone because of the area underneath the impactor is under through-thickness compression. A range of friction coefficients (0.3, 0.5, 0.75 and 0.9) were therefore used in simulation. The predicted delaminations in laminate  $[0_3/90_3]_s$  are shown in Figures 15 and 16. If the friction coefficient is low (0.3), a gap appears between the lobes of delamination in the early stage of damage or when the laminate is subject to a low energy impact, see Figure 15a. Subsequent to the early stage or a high energy impact, the damaged area expands in all directions with increase in pressure loading which causes the gap between the two delamination lobes to disappear. When the friction coefficient is equal to or greater than 0.5, the intact zone in the damage area can be captured for laminate  $[0_3/90_3]_s$  see contour plots in Figures 15b and 16.

The predicted delamination shapes of laminate  $[90_3/0_3]_s$  over the range of friction factor, 0.3, 0.5, 0.75 and 0.9 under three levels of impact energy are shown in Figure 17.

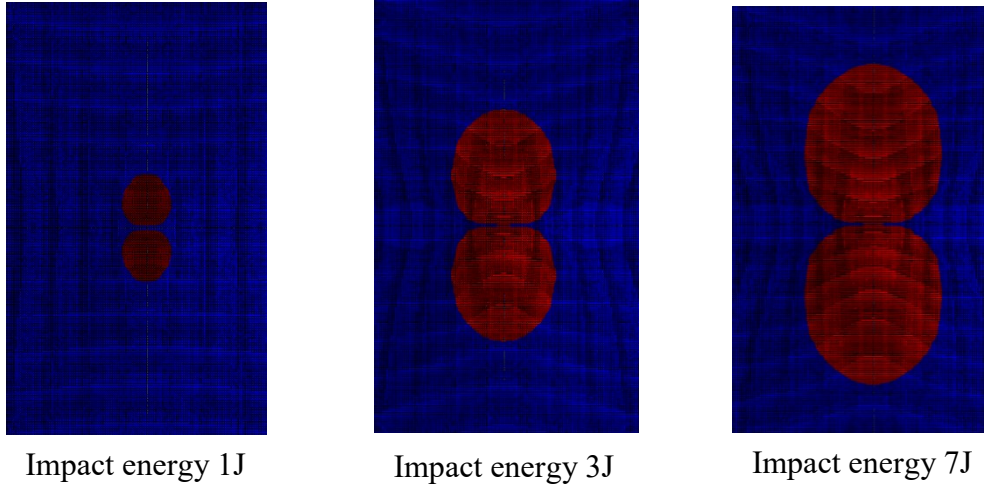
It is observed that high friction helps to separate the two delamination lobes, and when the friction coefficient is 0.9, the delamination lobes have completely separated, see Figure 17c. The simulation results match the experimental results of (Aymerich et al. 2009).

For both laminates  $[0_3/90_3]_s$  and  $[90_3/0_3]_s$ , the intact zone can be captured using the proposed method with different friction coefficients and enhancement factor 0.75. However, the gap size is relatively small compared to the intact zone which was measured in the experiments. This



was because of the lack of Hertzian contacts between the indenter and laminate (Sitnikova et al. 2017).

(a)



(b)

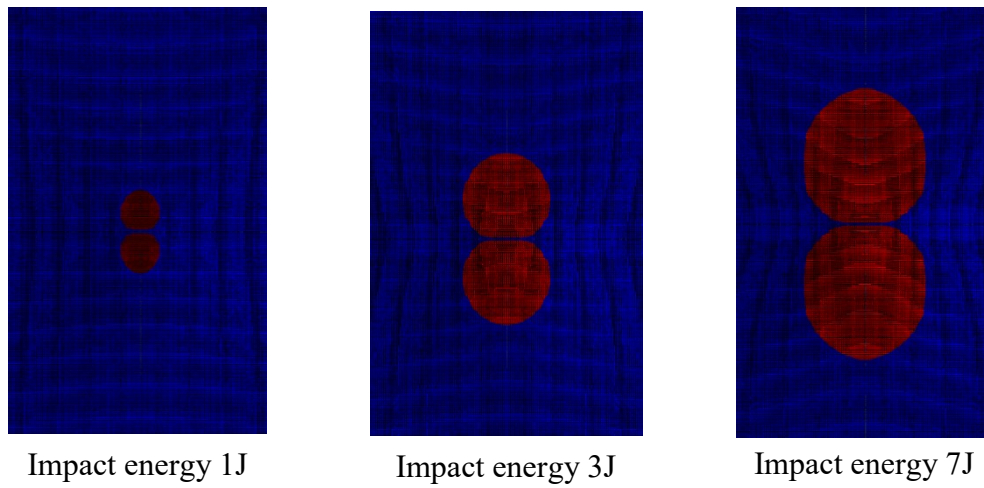
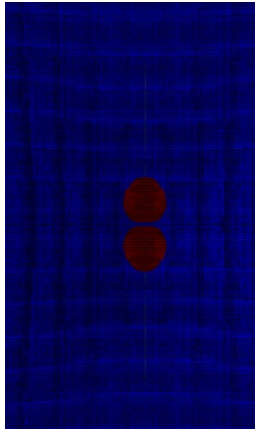
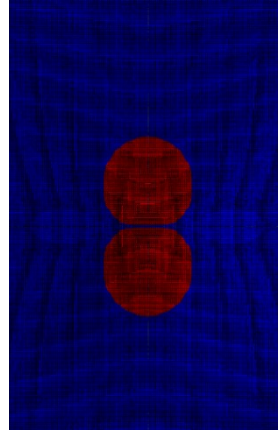


Figure 15 Effect of friction on predicted delamination in laminate  $[0_3/90_3]_s$  (a)  $f_c = 0.3$  and  $\eta = 0.75$  , (b)  $f_c = 0.5$  and  $\eta = 0.75$

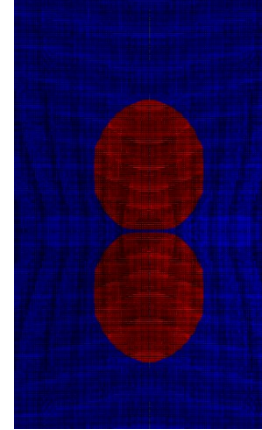
(a)



Impact energy 1J

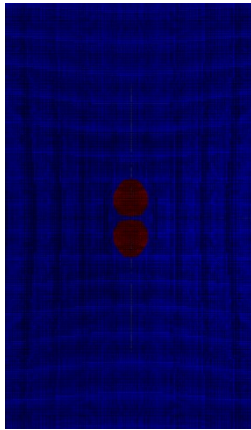


Impact energy 3J

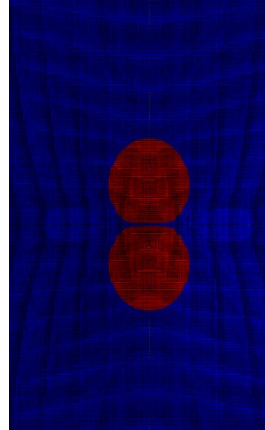


Impact energy 7J

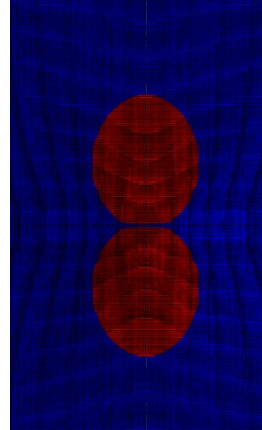
(b)



Impact energy 1J



Impact energy 3J



Impact energy 7J

Figure 16 Effect of friction on predicted delamination in laminate  $[0_3/90_3]_s$  (a)  $f_c = 0.75$  and  $\eta = 0.75$  , (b)  $f_c = 0.9$  and  $\eta = 0.75$

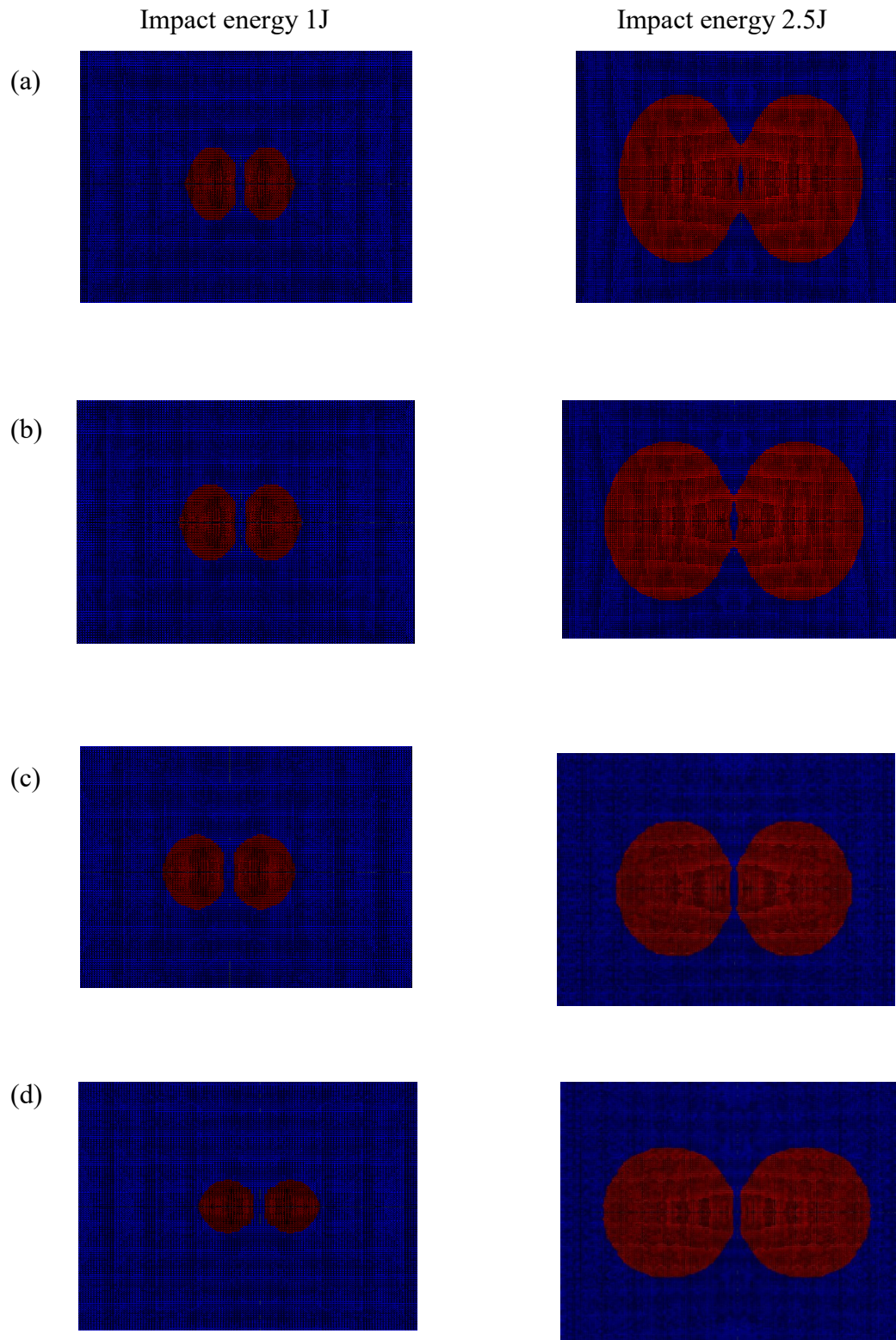


Figure 17 Effect of friction on delamination in laminate  $[90_3/0_3]_s$  (a)  $f_c = 0.3$  , (b)  $f_c = 0.5$  , (c)  $f_c = 0.75$  , and (d)  $f_c = 0.9$

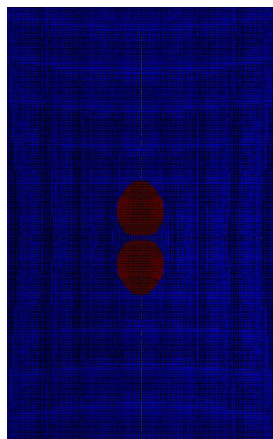


#### 4.4.3 Effect of Shear Strength Enhancement

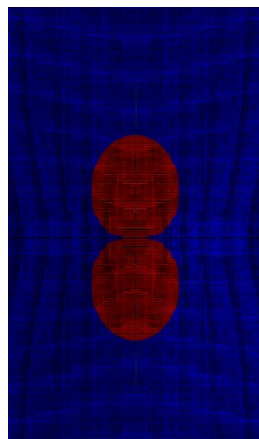
The through-thickness compression in the laminate underneath the indenter enhances the interlaminar strength and delays delamination initiation. Two shear strength enhancement factors (0.0 and 0.75) were used to show its influence on the delamination area. The simulated delamination shapes are shown in Figures 18 and 19.

If the shear strength enhancement is excluded ( $\eta = 0$ ), separate delamination lobes occur for the lowest energy level, 1 J, as clearly shown in Figure 18. With increase in impact energy, the delamination grows into the intact zone. When an enhancement factor 0.75 is used, the intact zone is present in the delamination area and remains there as the impact energy increases, as illustrated in Figure 19. Thus, it is evident that the shear strength enhancement should be taken into consideration to improve the numerical simulation.

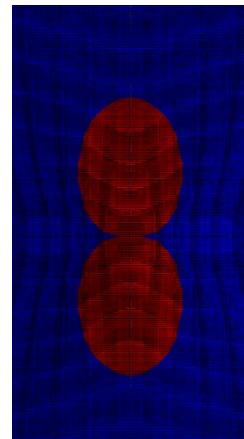
(a)



Impact energy 1J

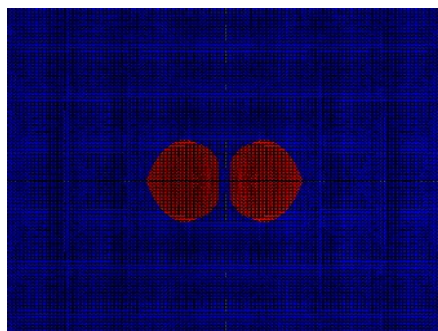


Impact energy 3J

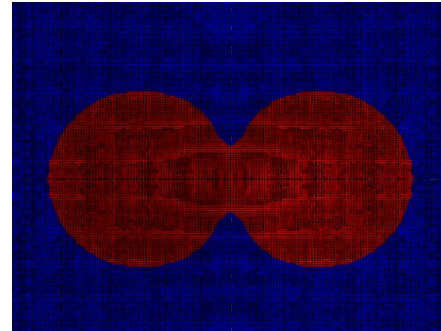


Impact energy 7J

(b)



Impact energy 1J



Impact energy 2.5J



Figure 18 Effect of enhancement factor ( $f_c = 0.75$  and  $\eta = 0$ ) on delamination (a) laminate  $[0_3/90_3]_s$  (b) laminate  $[90_3/0_3]_s$

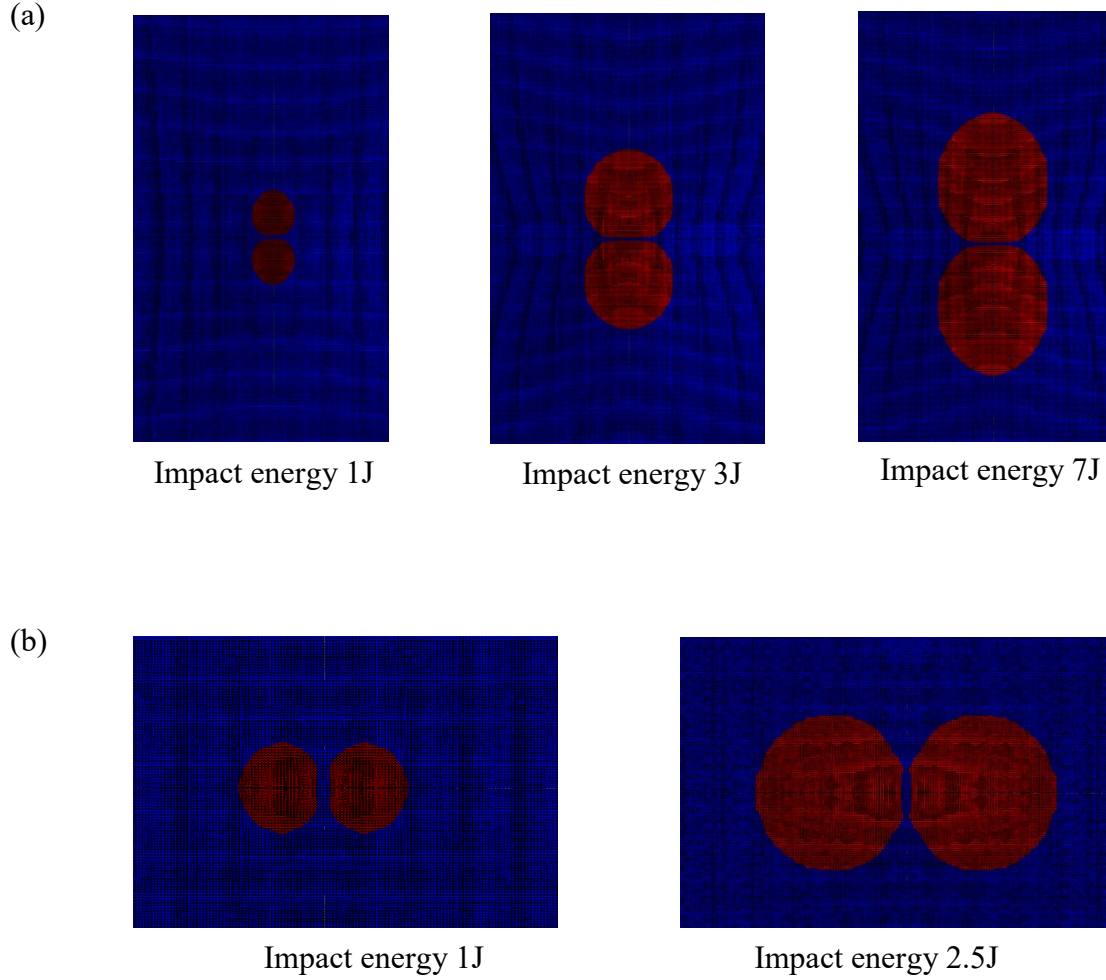


Figure 19 Effect of enhancement factor ( $f_c = 0.75$  and  $\eta = 0.75$ ) on delamination (a) laminate  $[0_3/90_3]_s$  (b) laminate  $[90_3/0_3]_s$

## 5. Conclusions

The cohesive and damage models developed and reported here were all implemented in ABAQUS via the User Subroutine UMAT. Numerical simulations of damage development in a composite laminate have been conducted. The predictions were compared with experimental results available in the literature to validate the proposed models. The followings finding were obtained.

- The experimental work reported in the literature has demonstrated that there is an intact zone immediately underneath the impactor, where there is no delamination when the

laminate is subjected to low velocity impact. This intact zone is successfully captured by the proposed model.

- The intact zone was captured when using the developed approach with enhancement factor ( $\eta=0.75$ ) and friction coefficient ( $f_c \geq 0.5$ ) for laminate  $[0_3/90_3]_s$ . However, a high value of friction (0.9) was required to separate the delamination lobes within the delamination area for laminate  $[90_3/0_3]_s$ .
- There is a strong interaction between matrix cracking and delamination in composite laminates. It is clearly observed that intra-laminar damage plays an important role in determining delamination shape. The intact zone between delamination lobes disappears when the matrix cracking is not taken into account, particularly at high impact energy levels.
- When the Hashin damage model for matrix cracking in ABAQUS is employed, no intact zone can be predicted. This demonstrates the advantage of the present proposed matrix cracking model over the Hashin's model in ABAQUS.

## References

- Aymerich, F., F. Dore, and P. Priolo. 2009. Simulation of multiple delaminations in impacted cross-ply laminates using a finite element model based on cohesive interface elements. *Composites Science and Technology* 69 (11-12):1699-1709.
- Du, D. D., Y. B. Hu, H. G. Li, C. Liu, and J. Tao. 2016. Open-hole tensile progressive damage and failure prediction of carbon fiber-reinforced PEEK-titanium laminates. *Composites Part B-Engineering* 91:65-74.
- Francesconi, L., and F. Aymerich. 2017. Numerical simulation of the effect of stitching on the delamination resistance of laminated composites subjected to low-velocity impact. *Composite Structures* 159:110-120.
- Guo, W., P. Xue, and J. Yang. 2013. Nonlinear progressive damage model for composite laminates used for low-velocity impact. *Applied Mathematics and Mechanics-English Edition* 34 (9):1145-1154.
- Hashin, Z. 1980. Failure Criteria for Unidirectional Fiber Composites. *Journal of Applied Mechanics-Transactions of the Asme* 47 (2):329-334.
- Linde, P., and H. de Boer. 2006. Modelling of inter-rivet buckling of hybrid composites. *Composite Structures* 73 (2):221-228.
- Liu, Y., B. Zwingmann, and M. Schlaich. 2014. Nonlinear Progressive Damage Analysis of Notched or Bolted Fibre-Reinforced Polymer (FRP) Laminates Based on a Three-Dimensional Strain Failure Criterion. *Polymers* 6 (4):949-976.
- Murugesan, N., and V. Rajamohan. 2017. Prediction of Progressive Ply Failure of Laminated Composite Structures: A Review. *Archives of Computational Methods in Engineering* 24 (4):841-853.
- Naderi, M., and M. M. Khonsari. 2013. Stochastic analysis of inter- and intra-laminar damage in notched PEEK laminates. *Express Polymer Letters* 7 (4):383-395.
- Sitnikova, E., S. G. Li, D. F. Li, and X. S. Yi. 2017. Subtle features of delamination in cross-ply laminates due to low speed impact. *Composites Science and Technology* 149:149-158.
- Y. Shi, C. P., C. Soutis. 2016. Low-velocity impact of composite laminates: Damage evolution. In *Dynamic Deformation, Damage and Fracture in Composite Materials and Structures*: Elsevier, 117–146.
- Zou, Z. M., and M. Hameed. 2018. Combining interface damage and friction in cohesive interface models using an energy based approach. *Composites Part a-Applied Science and Manufacturing* 112:290-298.